Effects of Steel Braces on Robustness of Steel Frames against Progressive Collapse

Kai Qian[1], M. ASCE, Xi Lan[2], Zhi Li[3], Feng Fu[4], C.Eng, F. ASCE

ABSTRACT

External installation of steel braces is one of the effective approaches to increase the lateral load resistance of the steel moment-resisting frames. However, the effects of existence of steel braces on the robustness of steel moment-resisting frames to resist progressive collapse is still not clear as little study has been carried out. To fill this gap, in this paper, six multi-story steel moment-resisting sub-frames (three bare frames and three braced frames) were fabricated and tested. Test results indicated that the specimen with reduced beam section in the connection zone performed best among three types of connections, due to the guaranteed formation of plastic hinges at the location of reduced section and avoiding brittle fracture of weld at the connection. Experimental results proved that steel braces could increase the load resisting capacity by 45.1% and 83.9% of the frame with weld connection and end plate connection, respectively. As the gusset plate restricted the rotation of the plastic hinges in the second story of the braced frames with V-shaped bracing, which decreased its deformation capacity and degraded its catenary action capacity. Actually, the ultimate load of the braced frames with V-shaped bracing is only 87.5% of that of the counterpart without any braces. As the compressive braces were severe buckled before the displacement reached 0.4% of the beam span, it has little effects on yield load but increases the initial stiffness of the bare frames. Thus, majority of the benefits of the bracing system were attributed into the tensile braces. Moreover, the analytical results evaluated the differences in load resistance and development of load resisting mechanisms in different stories. Furthermore, the contribution of compressive and tensile braces was de-composed individually by analytical analysis.

CE Database subject heading: progressive collapse; steel moment-resisting frame; braces; experimental, robustness

[1] Professor in College of Civil Engineering and Architecture at Guilin University of Technology, China, 541004, (corresponding author) qiankai@glut.edu.cn
[2]Research Student in College of Civil Engineering and Architecture at Guangxi University, China, 530004, lanx@st.gxu.edu.cn
[3] Research Fellow in College of Civil Engineering and Architecture at Guilin University of Technology, China, 531004, lizhi@st.gxu.edu.cn
[4] Senior Lecturer in Structural Engineering, School of Mathematics, Computer Science and Engineering, City, University of London, U.K., Feng.Fu.1@city.ac.uk

INTRODUCTION

Progressive collapse of steel frame structures may be triggered by the failure of one or couple vertical load bearing members in unintentional or intentional events. Majority of building codes only provide general recommendations, rather than detailed design provisions for progressive collapse. Recently, step by step design provisions were addressed by DoD (2010) and GSA (2013). Two major design methods are recommended: direct or indirect design methods. Among them, the alternate load path (ALP) method is commonly recommended as it is independent on the initial damage. ALP method focused on the ability of structures to bridge the lost column. Based on ALP method, extensive tests on steel beam-column connections or sub-assemblages were carried out by using column removal assessment method (Li et al. 2007; Sadek et al. 2011; Alashker et al. 2011; Dinu et al. 2016; Dinu et al. 2017; Liu et al. 2015; Tang et al. 2019; Dimopoulos et al. 2020; Qian et al. 2020; Wang et al. 2020). As the damage was concentrated in the beams or beam-column connections, rather than at the columns, it was recognized that the connections play a critical role in mitigating progressive collapse potential of the steel frames (Lew. et al. 2013, Yang and Tan 2013a, Yang and Tan 2013b). Lee et al. (2010) investigated the moment-axial force interaction of the double-span beams in steel frames under a column-missing scenario. It was found that the flexural action was the dominant mechanism at beginning. Due to buckling of the compressive flange and yielding of the tensile one, flexural action was slowly vanished with further increase of the displacement. When the displacement exceeded 10% of the beam span, the catenary action kicked-in and became the dominant mechanism in large displacement stage. To investigate the key design variables that influence the formation of catenary action, Khandelwal and El-Tawil (2007) carried out the numerical study of two steel joints subjected to the loss of a center column. Similar to the ones investigated by Khandelwal and El-Tawil (2007), Sadek et al. (2011, 2013) conducted the experimental study to provide insight into the behavior and

failure modes of steel beam-column connections, including the development of catenary action. Yang and Tan (2013a) tested seven beam-column sub-assemblages with different semi-rigid connections. It was concluded that the rotational capacity of the beam-to-column connections controlled the catenary action capacity. In summary, the connections in steel moment frames can be either rigid or semi-rigid connections. The use of rigid connections is the primary option for frames with medium or high ductility demands in earthquake design. However, semi-rigid connections are also allowed (AISC 2005a). Therefore, it is of interest to evaluate whether rigid or semi-rigid connections can provide sufficient strength and ductility to resist progressive collapse.

Catenary action, as the second defense line, is possible to increase the load resisting capacity of moment resisting frames significantly (Deng et al. 2020; Qian et al. 2021a). However, for steel moment-resisting frames configurated under non-seismic design principles, irregular layout or long span may prone to progressive collapse. Pantidis and Gerasimidis (2017, 2018) pointed out that two possible collapse mechanisms caused by the loss of a column scenario, the yielding type (beam plasticization) or the stability (column buckling) failure mode. Other modes of collapse could be the shear failure of the beam-to-column connections (Khandelwal and El-Tawil 2011). In recent years, progressive collapse events were occurred continuously, such as the collapse of twin towers in World Trade Center in New York, collapse of steel frame at Argyle High School in Texas, or the collapse of steel frame at Jiaxin Hotel in Quanzhou, China. Thus, it was necessary to look for additional load resistance to upgrade the ability of steel frames to mitigate progressive collapse. Galal and El-Sawy (2010) discussed the enhancement of three retrofit strategies on mitigating progressive collapse risks. The post-tensioned (PT) steel frames, are evidenced well robustness under strong earthquakes (Ricles et al. 2001; Christopoulos et al. 2002; Garlock et al. 2005; Pirmoz and Liu 2016; Moradi and Alam 2017). Although steel bracing system was able to provide satisfactory seismic resistance of steel frames (AISC 2005a; AISC 2005b), the effects of steel bracing to resist progressive collapse are still unclear. The numerical analyses by Khandelwal et al. (2009) showed that seismically designed steel braced frames could sustain the sudden loss of a column without collapse as steel braces improved the robustness significantly. However, little tests had done in this area. Chen et al. (2012) found that the

horizontal braces could upgrade the load resistance of steel frames to mitigate progressive collapse. It was indicated that the horizontal braces formed additional ALP and transferred partial of the vertical loads to adjacent columns directly, which could enhance the vertical load resistance significantly.

Additionally, previous tests were mainly based on specimens of single-story beam-column sub-assemblages or connections. It is simply assumed that each story has identical geometric and material properties and thus, assuming each story performed identically. However, as pointed out by Qian et al. (2020), Qian et al. (2021b), and Weng et al. (2020), the load resistance of the beams in the first story is quite different to the second and upper stories. It could be explained that the interaction among different stories, which leads to different mobilization of load resisting mechanisms (flexural and catenary action). Thus, to deep understand the behavior of steel frames subjected to column loss scenarios, six two-story steel sub-frames using either rigid or semi-rigid connections are tested by push-down loading regime in the present study. Based on experimental and analytical results, the effects of steel braces with various configurations are quantified. The contribution of compressive and tensile braces is de-composed individually. Furthermore, as mentioned above, the different behavior of the structural members in different stories is also quantified.

EXPERIMENTAL PROGRAM

Test specimens

As shown in Fig. 1, a six-story, 6×6 bay prototype steel frame was seismically configurated and fabricated in accordance with AISC-341 (2005a). This prototype frame was presumed to be located on a D class site (stiff soil profile), with correspondent acceleration parameters S_{DS} and S_{D1} of the design response spectrums are 0.20 and 0.14, respectively. The story height of the prototype frame is 3.0 m with span length of the frame in longitudinal and transverse direction was 8.4 m by 6.0 m, respectively. The designed dead and live loads are 5.1 kN/m^2 and 3.0 kN/m^2, respectively. Given the capacity limitation of test facilities, only 1/2-scaled models were fabricated. To well simulate horizontal restraints from the surrounding bays, beams were extended with length of 655 mm beyond the side column, as shown in Fig. 2a. As described below, a horizontal chain-pole would be installed to connect the overhanging beam and A-frame.

As listed in Table 1, the six specimens included three steel moment-resisting frames without any braces (WB, EB, and RB) and three counterparts with extra bracing system (WX, EX, and RV). Different connections were employed, the numeric alphabetics W, E, and R represent welded connection, end plate connection, and reduced beam section connection, respectively. Additionally, the numeric alphabetic X and V represent X-shaped bracing and V-shaped bracing, respectively. As shown in Fig. 3, for welded connection, the flange and web of beam were welded to column flange using complete joint penetration welds. For end plate connection, the beam flanges and web were connected to a 10 mm thick end plate by same type of welds, while the end plates were fixed to the column flange by six rows of Grade 8.8 M18 bolts. Bolts were preload of 345 N·m, which was applied by a torque wrench. For reduced beam section connection, similar to welded connection, except, the beam flanges, at a distance of 70 mm from the column flange, was cut in a circular manner, as shown in Fig. 3c. Section HN 200×100×5.5×8 was used for beams whereas HW 150×150×7×10 was for columns. Continuity plates in the column joint was designed with thickness of 10 mm.

The braced frames have identical dimension and detail as corresponding bare frames, except extra bracing system with different configurations were installed at the second story. The braces and their connections were also designed according to AISC (2005a). The braces are welded and connected to the beam flanges through a gusset plate. The gusset plate was designed to be stronger than the braces to avoid yielding or fracture occurring at the gusset plate (Khandelwal et al. 2009; AISC (2005a)). The force acting on the weld was determined by the uniform force method (Richard 1986). Taking WX and RV as an example, as shown in Fig. 2a, the brace was an angle steel with dimensions of 36 ×36 × 4 mm. X braces were eccentrically installed at WX and EX, the gusset plate was a steel plate with the size of 330×125×12 mm. Moreover, V braces were installed at RV, the gusset plates with the size of 160×155×12 mm were fixed at the beams in the second story while the bottom one with size of 510×155×12 mm was installed at the middle span of the beams in the first story.

Material properties

Grade Q235 steel is used for column, beam, and angle. The measured yield strength, ultimate strength, and elongation of the angle and structural components are tabulated in Table 2. As no

independent coupon test was conducted for bolts (Grade 8.8 M18), the yield strength and ultimate strength of the bolts are provided by the supplier.

Test setup

As illustrated in Fig. 4, the bottom of each side column was pin supported. Each overhanging beam beyond the side column was connected to the A-frame via a horizontal chain-pole (Item 6 in Fig. 4). The middle column in ground story was removed prior to applying concentrated load to replicate the scenario of missing a middle column. The load was applied by a hydraulic jack (Item 1 in Fig. 4) at the top of middle column by a displacement-controlled method. To avoid undesired out-of-plane failure, a steel assembly (Item 3 in Fig. 4) was installed beneath the hydraulic jack (Item 1 in Fig. 4). Moreover, hydraulic jack (Item 4 in Fig. 4) together with self-balance loading system was used to simulate axial force of side column with the ratio of axial compressive force of 0.3.

Instrumentations

The layout of instrumentations is shown in Fig. 4. A load cell (Item 2 in Fig. 4) was installed below the hydraulic jack (Item 1 in Fig. 4) to measure the applied concentrated load. Tension/compression load cell (Item 7 in Fig. 4) was installed at each horizontal chain-pole (Item 6 in Fig. 4) to measure its horizontal reaction force. A load pin (Item 8 in Fig. 4) was installed at each pin support to measure the reaction force of the bottom pin support. In addition, a series of linear variable differential transformers (LVDTs) (Item 5 in Fig. 4) were installed along the beam span or column height to measure the beam deformation shape and column lateral drift, as shown in Fig. 4.

As shown in Fig. 2, the strain at critical sections was monitored by a series of strain gauges or strain gauge rosettes. Thus, the internal force of the beam and brace could be determined by simplified section analysis.

EXPERIMENTAL RESULTS

Six two-story sub-frames were tested to quantify the effects of steel braces to enhance robustness of steel frames. The key results are listed in Table 3. As the results of WB and RB had been introduced in Qian et al. (2020) in detail, only the main characteristics of these two specimens were addressed

herein. The different behavior of bare frames and counterpart braced frames was the main concern in the present study.

Global behavior

WB: As shown in Fig. 5a, its yield load of 147.8 kN was measured when the middle column displacement (MCD) reached 45 mm. Therefore, the initial stiffness, which is defined as the ratio of yield load to corresponding yield displacement, was 3.3 kN/mm. At the MCD of 200 mm, WB reached its ultimate load of 197.5 kN, which is defined as the peak load resistance. Afterwards, the load resistance of WB began to drop slowly due to weld fracture occurred at the connections in the first story. However, when MCD reached 281 mm, the load resisting capacity began to re-ascend due to the catenary action developed in the second story. With the increase of the vertical displacement to 377 mm, the weld fracture occurred at the beam web near the middle column in the ground story. Further increasing the MCD to 410 mm, the welding at the beam end near middle column in the second story fractured completely. Its failure mode is shown in Fig. 6.

WX: The compressive braces of the X bracing system began to buckle at the beginning of the test, which means the compressive braces may not be so effective to provide additional alternate load path of the specimen, which will be further confirmed in the section of analytical analysis. However, when the MCD reached 11.2 mm (0.4% of the beam span), the buckling of compressive braces become severe. Thus, they have little contribution for yield load enhancement as the yield load of 233.9 kN was measured at a MCD of 31 mm. This will be further confirmed by following analytical results. The initial stiffness was 7.5 kN/mm, which is 227.3% of that of WB. At a MCD of 137 mm, the tensile brace in the left bay fractured. When the displacement increased to 221 mm, weld fracture both occurred at the connections near the side column in the ground story and the middle column in the second story. Actually, the weld fracture accompanied by considerable decrease of the load resistance. The load-displacement curve kept increasing until weld fracture occurred at the connection near side column in the ground story at a MCD of 311 mm. WX reached its ultimate load of 286.5 kN, which was 145.1% of WB, at the MCD of 382 mm as complete weld fracture occurred at the connection near left side column in the ground story. However, the load resistance did not lose completely owing to the

catenary action developed in the second story, regardless the loss of load resistance of the entire first story. Further increasing the MCD, the complete fracture occurred at the connection near the middle column in the second story. The failure mode of WX is shown in Fig. 7. Fracture occurred in the tensile brace. Severe out-of-plane buckling was observed in compressive braces. No yielding was observed in the gusset plates. However, although the failure mode of the connections in WX is generally similar to that of WB, the fracture of the connections near the side column was more severe than that near the middle column.

EB: As shown in Fig. 5b, the yield load of 94.4 kN was measured at a MCD of 42 mm. Thus, the initial stiffness was 2.2 kN/mm, which was only 66.7% of that of WB. However, EB exhibited more flexibly than that of WB. Thus, the load resistance kept increasing until weld fracture occurred at the connection in the second story at a MCD of 452 mm. EB reached its ultimate load of 255.4 kN at a MCD of 515 mm. The failure mode of EB is shown in Fig. 8. Similar to WB, the weld fracture occurred at Joint A.

EX: The yield load of 148.5 kN was observed at a MCD of 30 mm, which is about 157.3% of that of EB. Thus, the initial stiffness was 5.0 kN/mm. The tensile braces in the right bay fractured at a MCD of 320 mm. Further increasing MCD to 407 mm, the bolts in the connection near the side column fractured. However, the load resistance rapidly recovered after shortly decrease. The weld fracture occurred near the middle connection in the second story at a MCD of 450 mm. Subsequently, bolts in the top row of this connection fractured at the MCD of 467 mm. However, the load resistance was able to increase sustainably until the test was stopped due to reaching stroke capacity of the jack. The ultimate load of 469.8 kN was measured at a MCD of 526 mm. The failure mode of EX is shown in Fig. 9. Similar to WX, fracture occurred in the tensile brace and severe buckling was observed in the compressive braces. The connections failed either in bolt fracture or weld fracture. The 45 degrees full-slant fracture surface of the bolts indicated that the bolts were suffered both tension and shear. Different to EB, although weld fracture was also observed in EX, it did not propagate into the web. Thus, the braces increased the deformation capacity of EX significantly.

RB: As shown in Fig. 5c, for RB, the yield load of 106.8 kN was measured at a MCD of 37 mm. Thus, the initial stiffness was 2.9 kN/mm, which was only 87.9% of that of WB. For RB, the plastic hinges were formed at the center of reduced beam section, which prevented the early fractures at the welded connection. RB reached its ultimate load of 407.0 kN, which was 206.1% of WB, at the MCD of 468 mm. Its failure mode is shown in Fig. 10.

RV: The yield load of 165.2 kN, which is about 154.7% of that of RB, was measured at a MCD of 30 mm. Thus, the initial stiffness was 5.5 kN/mm. Before the tensile braces fractured, the weld fracture already occurred at the connection near the middle column in the second story. Different to RB, the fracture occurred near the weld connection rather than the reduced beam section due to the gusset plates strengthened the reduced section of the beam in the second story. At the MCD of 253 mm, the tensile brace in the left bay was fractured. At the MCD of 421 mm, RV reached its ultimate load of 356.3 kN before the weld fractured completely. The deformation capacity was only 90.0% of RB, as the V braces strengthened the zone of plastic hinges in the beam of second story, which restricted the rotation of the plastic hinge. The failure mode of RV is shown in Fig. 11. Similarly, fracture occurred in the tensile brace while severe buckling occurred in the compressive braces. The weld fracture occurred in Joint A. The V braces are welded on one side of the gusset plate and the brace forces were not along the center axis of the beam, which resulted in torsional failure of the beams. The buckling occurred at point D. The torsion mainly concentrated between beam segment CD leading to the tear failure occurred at Joint B.

Horizontal reaction force

Fig. 12 decomposes the contribution of horizontal reaction force at the right side. Negative values represent compressive force whereas positive values mean tensile force. As shown in Fig. 12, at small deformation stage, the compressive reaction force of total reaction force was mainly provided by the bottom pin support. The maximum compressive reaction force in WB, WX, EB, EX, RB, and RV was -24.7, -7.8, -35.8, -23.5, -31.9, and -22.1 kN, respectively. With further increasing the displacement, the compressive force began to decline and transferred into tension. However, the tensile force from the bottom pin support kept marginal in catenary action stage and majority of tensile reaction force was

provided by the horizontal chain-poles connected to the overhanging beams. As shown in Figs. 12a, c, and e, for bare frames, the tensile force was equally from the ground story and second story, although the pre-mature failure occurred at the ground story of WB. Conversely, as shown in Figs. 12b, d, and f, for braced frames, the tensile force from the second story was larger than that from the ground one. The maximum tensile reaction force of WB, WX, EB, and EX was 363.5 kN, 406.8 kN, 551.5 kN, and 835.8 kN, respectively. Thus, contrary to compressive forces, with the help of braces, greater tensile reaction force and catenary action was developed in braced frames. However, the maximum tensile reaction force of RB and RV was 875.9 kN and 462.8 kN, respectively. This could be explained at the gusset plate restricted the rotation of plastic hinges of the beams in the second story of RV, which prevented the development of catenary action.

Deformation measurements

The deformation shape of edge column was shown in Fig. 13. It should be noted that the positive value and negative value represents inward and outward movement, respectively. As shown in Fig. 13a, for WB, initially, the horizontal inward movement was observed at the beam-column joints. However, the horizontal inward movement at the joint in the second story was much larger than that in the ground story. The maximum horizontal inward movement of the joint in the first and second story was only 3.2 mm and 9.1mm, respectively. As shown in Fig. 13b, for WX, outward movement was initially measured in the ground story. The outward movement began to decrease when the vertical displacement exceeded 60 mm. This is because the compressive brace generated additional outward movement in the ground floor. However, the tensile braces are prone to pull the joint in the second floor inward. The maximum inward movement of joint in the first and second stories was 4.3 mm and 15.2 mm, respectively. Similar results were observed for other specimens.

Internal force measurements

To further understand the load resisting mechanism of frames and de-composite the load contribution of braces, the internal forces in beams and braces were quantified individually. The reliability of strain gauge results to determine the load resistance of the specimens was evaluated first. The vertical force and horizontal reaction force of braced specimens were determined by Eqs.1 and 2:

$$F_V = F_{V-Frame} + F_{V-Brace} \quad (1)$$

$$F_H = F_{H-Frame} + F_{H-Brace} \quad (2)$$

where F_V and F_H are the vertical force and horizontal reaction force of braced frame; $F_{V-Frame}$ and $F_{H-Frame}$ are the vertical force and horizontal reaction force of the bare frame, which has been described in detail in authors' previous work (Qian et al. 2020); $F_{V-Brace}$ and $F_{H-Brace}$ are the vertical force and horizontal reaction force provided by braces.

For X bracing configuration, the vertical and horizontal component force from braces could be calculated by Eqs. 3 and 4, respectively. However, for V bracing configuration, the force of braces could not be equivalent into the load resistance at the middle column directly. A schematic diagram was presented to illustrate the relationship, as shown in Fig. 14 and Eq. 5.

$$F_{V-Brace}=2\left(N_T \sin\alpha - N_C \sin\beta\right) \quad (3)$$

$$F_{H-Brace}=2\left(N_T \cos\alpha + N_C \cos\beta\right) \quad (4)$$

$$N_T'=N_T \cos\theta \quad (5)$$

where N_T and N_C are the axial force of the tensile and compressive brace, respectively; α is the angle between tensile brace and horizontal axis; β is the angle between compressive brace and horizontal axis; N_T' is the adopted axial force of tensile brace for RV; θ is the angle between tensile brace and diagonal line.

The axial force of braces can be calculated according to Eq. 5.

$$N = EA\left(\sum_{i=1}^{n}\varepsilon_i\right)\Big/n \quad (6)$$

where E is the elastic modulus; A is the section area of the brace; $\left(\sum_{i=1}^{n}\varepsilon_i\right)\Big/n$ is the average axial strain of the cross-section.

Fig. 15 compares the vertical load-displacement curve and horizontal reaction force-displacement curve based on load cell results and strain gauge results. From the figures, it can be seen that the analytical results based on strain gauge generally agree with the load cell results well. Thus, the

analytical results based on strain gauge results were used in following analysis and discussion. Fig. 16 illustrates the de-composition of the load resistance from the frame and steel braces. As shown in the figures, the load resistance from steel braces was higher than that from frame initially. However, the load resistance of the frame kept increasing due to the development of flexural action. Conversely, the load resistance from braces began to reduce soon due to compressive braces buckled. When partial of the tensile brace fractured, the contributions of steel braces are reduced to 37.7%, 38.5%, and 29.5 % for WX, EX, and RV, respectively.

DISCUSSION OF TEST RESULTS

Effects of connection types

Fig. 17 compares the behavior of different connections. As shown in Fig. 17a, for bare frames, the greatest load resisting capacity was measured in RB due to the reduced section prevents the pre-mature fracture of the welds. Thus, it can be concluded that, when properly designed and fabricated, reduced beam section connections can be a cost-effective solution to enhance the robustness of steel frames with rigid connections. The second largest capacity was observed in EB. Among these three tests, EB achieved the greatest deformation capacity. Although the failure modes of EB are also controlled by weld fracture, it has a more ductile process. Before weld failure, the end plate yielded and experienced considerable local plastic deformation, which brought in greater catenary action capacity. The load resistance from flexural action and catenary action are compared in Figs. 17b and c, respectively. As shown in Fig. 17b, WB has the greatest flexural action capacity. At flexural action stage, WB reached the largest initial stiffness and load resistance. As shown in Fig. 17c, when catenary action is included in the load resistance, the load resisting capacity could increase significantly especially for RB and EB.

Effects of braces

As shown in Fig. 5 and Table 3, the measured yield load of WB, WX, EB, EX, RB, and RV were 147.8, 233.9, 94.4, 148.5, 106.8, and 165.2 kN, respectively. Thus, the X bracing system increased the yield load of WB and EB by 58.3% and 57.3%, respectively. Similarly, the V bracing system increased the yield load of RB by 54.7%. Regarding the initial stiffness, WB, WX, EB, EX, RB and RV were

3.3, 7.5, 2.2, 5.0, 2.9, and 5.5 kN/mm, respectively. Thus, the X bracing system increased the initial stiffness of WB and EB by 127.3% and 120.2%, as the X bracing system in WB and EB could transfer partial of the vertical load to the side column directly. Similarly, the V bracing system increased the initial stiffness of RB by 89.7%. The ultimate load capacities of WB, WX, EB, EX, RB, and RV in the large deformation stage were 197.5, 286.5, 255.4, 469.8, 407.0, and 356.3 kN, respectively. WX and EX could increase the ultimate load capacity of the counterpart bare frames by 45.1% and 83.9%. This could be explained as one of tensile braces in WX and EX were not fractured until test stopped, which increased the load resistance in catenary action stage. Conversely, RV only achieve 87.5% of the ultimate load capacity of RB. This is because the gusset plate of RV bracing system in the second story restricted the rotation of plastic hinges, which was designated to form at the reduced section. Thus, the catenary action capacity and deformation capacity of RV was even less than RB. Moreover, it should be noted that for a steel frame, only partial of peripheral structural bays have bracings. Thus, the effects of bracings mentioned above are only suit for these braced bays.

Contribution of load resisting mechanisms

Fig. 18 gives the de-composition of load resistance of frame from catenary action and flexural action. As shown in Fig. 18a, before MCD reached 128 mm, significant bending moment was developed and thus, flexural action dominated the load resistance of WB at the beginning of the test. In large deflection stage, axial tensile force and catenary action was mobilized. Flexural action and catenary action worked together to redistribute the applied load. The maximum flexural action and catenary action were 175.5 kN and 78.7 kN, respectively. For WX, flexural action was higher than that of WB before weld fracture occurred. Different to WB, the vertical load of frame could keep increasing until reached its maximum load resistance due to the significant catenary action. Due to X braces, the flexural action and catenary action were increased by 17.8% and 61.3%, respectively. As shown in Fig. 18c, although the maximum flexural action was only 74.1% of that of WB, the catenary action was 207.1% of that of WB. Thus, the ultimate load of EB is 129.3% of that of WB. For EX, it is worth noting that significant tensile force was developed in the beams. Due to X braces, the flexural action and catenary action was increased by 25.7% and 137.9%, respectively. As shown in Fig. 18e, although

both WB and RB were welded connection, greater catenary action was developed in RB. This is because the failure of WB was controlled by weld fracture, which was brittle and pre-mature. The reduced beam section would avoid this brittle failure and increase the ductility and deformation capacity. Although the maximum flexural action was only 82.1% of that of WB, the catenary action of RB was 380.8% of that of WB and thus, the ultimate load of RB is 203.9% of that of WB. As shown in Fig. 18f, RV sustained substantial bending moment before the connection fractured. However, with further increasing the displacement, the increase of catenary action was limited, which was unlike RB. This is mainly due to gusset plates at the second story prevents the development of catenary action. Comparing with RB, the flexural action and catenary action was 115.6% and 55.8% of its counterpart.

Fig. 19 decomposes the load resistance from the first and second stories. It can be seen that the trend of load resistance from the first and second story is similar before failure first occurred at the connection. However, the load resistance from the ground story was slightly larger than that from the second story due to different horizontal constraints. To further study on the difference, as labeled in Fig. 20, the flexural and catenary action of each story were extracted. Due to higher rotational restraints from the side column, the flexural action from the first story may be larger than that of second story. In the first story, the catenary action developing in the beams is always in tension. However, the catenary action of the second story is in compression (negative) firstly, and then transfers into tension at the large deformation stage. Therefore, both flexural and catenary action could develop in the first story effectively, leading to larger resistance.

De-composition of the load resistance from braces

Fig. 21 gives the de-composition of contribution of braces from tensile and compressive braces. For WX, EX, and RV, the maximum load resistance of steel bracing was 111.9, 120.3, and 87.1 kN, respectively. As shown in the figures, WX and EX could keep increasing after buckling of compressive brace. These two specimens reached their maximum value when the one of the tensile braces fractured. Before buckling of the compressive brace, the maximum load resistance from compressive brace of WX and EX were 19.2 kN and 19.1 kN, respectively. Different to WX and EX, after buckling of the compressive braces, RV reached its maximum value as large part of the load resistance provided by

the compressive braces. For RV, the maximum load resistance from compressive brace was 51.7 kN, which was 269.2% and 270.7% of that of WX and EX, respectively. However, as shown in in Fig. 21, due to the buckling of the compressive braces at very early stage, they only affect the initial stiffness significant. To further understand the contribution of steel braces, the axial force of tensile and compressive braces was determined and presented in Fig. 22. From basic analysis, the yield load and ultimate load of the tensile braces were determined as 85.6 kN and 115.9 kN, respectively. Tensile braces in X configuration could achieve their yield load and even achieved their ultimate load before fracture. However, the tensile braces in V configuration only achieved their yield load. From basic analysis, the buckling load of compressive brace were 23.0 kN and 57.6 kN for X and V configuration, respectively. As shown in the figures, the compressive braces in X configurations could achieve their buckling load. Different to X configuration, the compressive braces in V configuration could not achieve their buckling load.

CONCLUSIONS

To evaluate the effects of steel braces on the behavior of steel frames to mitigate progressive collapse, six two-story steel sub-frames (three bare frames and three braced frames) with different connections were tested under a middle column missing scenario. Based on experimental results, following conclusions are drawn:

1. The results from bare frames revealed that various of failure mode, ductility, and load resisting mechanisms were developed in the steel frames with different types of connections. Different to weld fractures in WB and EB, RB failed by fracture at the reduced beam section. Thus, the greatest deformation capacity and catenary action capacity were achieved in RB. The ultimate load capacity of RB was 206.1% and 159.4% of that of WB and EB, respectively.
2. The test results demonstrated that for WB, the main load resistance was from the flexural action, rather than catenary action, which is mainly due to pre-mature weld fracture at the connections. Conversely, for EB and RB, relatively less flexural action was developed, catenary action increased the load resisting capacity of EB and RB by 81.6% and 125.8%, respectively. Thus, the load resistance of these two connections were dominated by catenary action, rather than flexural

action.

3. The test results indicated that steel braces could provide considerable additional load resistance for steel frames to resist progressive collapse effectively. The steel braces in WX, EX, and RV increased their initial stiffness by 127.3%, 120.2%, and 89.7%, respectively. For RV, the effectiveness of the steel braces is relatively milder because their braces could not transfer the vertical load to side columns directly. The X brace in WX and EX increased the ultimate load capacity of the bare frames by 45.1% and 83.9%. However, the V braces in RV even decreased the ultimate load capacity of RB by 12.5% as the gusset plates restricted the formation of plastic hinges in reduced beam section. Thus, the gusset plate should not be installed in the reduced beam section to avoid negative effects on braced specimens, as the gusset plate may restrict the rotation capacity of the reduced beam section.
4. The out-of-plane buckling of compressive braces occurred from the beginning of the test, which could not provide sufficient load resistance after buckling, especially for X bracing system. However, due to the difficulties in predicting the location of column missing accurately, a symmetric bracing configuration is still recommended. As the additional load resistance mainly attributed into the tensile braces, the fracture of tensile braces normally accompanied by the drop of load resistance significantly. From the failure modes, it was found that the braces may change the failure mode of the beams as the beam ends may suffer greater shear force, which may lead to pre-mature weld fracture or bolt fracture. It should be noted that above conclusions regarding steel braces are only suit for the structural bays with steel bracings. For the structural bays without any bracings, the benefits of bracings could not be incorporated in design or analysis.

DATA AVAILABILITY

Some or all data, models, or code that support the findings of this study are available from the corresponding author upon reasonable request.

ACKNOWLEDGEMENTS

This research was supported by a research grant provided by the Natural Science Foundation of China (Nos.52022024, 51778153). Any opinions, findings and conclusions expressed in this paper are those of the writers and do not necessarily reflect the view of Natural Science Foundation of China.

REFERENCES

AISC 2005a. Seismic Provisions for Structural Steel Buildings. ANSI/AISC 341-05. Chicago: AISC.

AISC 2005b. Specifications for Structural Steel Buildings. ANSI/AISC 360-05. Chicago: AISC.

Alashker, Y., and Li, H. H., El-Tawil, S. (2011). "Approximations in Progressive Collapse Modeling." J. Struct. Eng, 137 (9): 914-924.

Chen, J., Peng, W., and Ma, R. (2012). "Strengthening of Horizontal Bracing on Progressive Collapse Resistance of Multistory Steel Moment Frame." J. Perform. Constr. Facil. 26: 720-724.

Christopoulos, C., Filiatrault, A., Uang, C. M., and Folz, B. (2002). "Posttensioned Energy Dissipating Connections for Moment-Resisting Steel Frames." J. Struct. Eng. 128 (9): 1111-1120.

Deng, X. F., Liang, S. L., Fu, F., and Qian, K. (2020) "Effects of High-Strength Concrete on Progressive Collapse Resistance of Reinforced Concrete Frame", J. Struct. Eng. 146(6): 04020078.

Dimopoulos, C. A., Freddi. F., Karavasilis, T. L., and Vasdravellis, G., (2020). "Progressive Collapse Resistance of Steel Self-Centering MRFs Including the Effects of the Composite Floor." Eng. Struct. 206: 110143.

Dinu, F., Marginean, I., and Dubina, D. (2017). "Experimental Testing and Numerical Modelling of Steel Moment-Frame Connections under Column Loss." Eng. Struct. 150: pp. 861-878.

Dinu, F., Marginean, I., Dubina, D., and Petran, I. (2016). "Experimental Testing and Numerical Analysis of 3D Steel Frame System under Column Loss." Eng. Struct. 113: 59-70.

DoD (2010). "Design of Building to Resist Progressive Collapse." UFC 4-023-03. Washington, DC, USA.

Galal, K., and El-Sawy, T. (2010). "Effect of Retrofit Strategies on Mitigating Progressive Collapse of Steel Frame Structures." J. Constr. Steel Res. 66 (4): 520–531.

Garlock, M. M., Rides, J. M., and Sause, R. (2005). "Experimental Studies of Full-Scale Posttensioned Steel Connections." J. Struct. Eng. 131 (3): 438-448.

GSA (2013). “Progressive Collapse Analysis and Design Guidelines for New Federal Office Buildings and Major Modernization Projects.” Washington, DC, USA.

Khandelwal, K., and El-Tawil, S. (2007). “Collapse Behavior of Steel Special Moment Resisting Frame Connections.” J. Struct. Eng. 133 (5): 646-655.

Khandelwal, K., and El-Tawil, S. (2011). “Pushdown Resistance as a Measure of Robustness in Progressive Collapse Analysis.” Eng. Struct. 33(9):2653-2661.

Khandelwal, K., El-Tawil, S., and Sadek, F. (2009). “Progressive Collapse Analysis of Seismically Designed Steel Braced Frames.” J. Constr. Steel Res. 65 (3): 699-708.

Lee, C. H., Kim, S., and Lee, K. (2010). “Parallel Axial-Flexural Hinge Model for Nonlinear Dynamic Progressive Collapse Analysis of Welded Steel Moment Frames.” J. Struct. Eng. 136 (2): 165-173.

Lew, H. S., Main, J. A., Robert, S. D., Sadek, F., and Chiarito, V. P. (2013). “Performance of Steel Moment Connections under a Column Removal Scenario. I: Experiments.” J. Struct. Eng. 139 (1): 98-107.

Li, L., Wang, W., Chen, Y. Y., and Teh, L. H. (2007). “Column-Wall Failure Mode of Steel Moment Connection with Inner Diaphragm and Catenary Mechanism.” Eng. Struct. 131: 553-563.

Liu, C., Tan, K. H., and Fung, T. C. (2015). “Investigations of Nonlinear Dynamic Performance of Top-And-Seat with Web Angle Connections Subjected to Sudden Column Removal.” Eng. Struct. 99: 449-461.

Moradi, S., and Alam, M. S. (2017). “Lateral Load-Drift Response and Limit States of Posttensioned Steel Beam-Column Connections: Parametric Study.” J. Struct. Eng. 143 (7): 4017044.

Pantidis, P., and Gerasimidis, S. (2017). “New Euler-Type Progressive Collapse Curves for Steel Moment-Resisting Frames: Analytical Method.” J. Struct. Eng. 143 (9): 04017113.

Pantidis, P., and Gerasimidis, S. (2018). “Progressive Collapse of 3D Steel Composite Buildings under Interior Gravity Column Loss.” J. Constr. Steel Res. 150:60-75.

Pirmoz, A., and Liu, M. M. (2016). “Finite Element Modeling and Capacity Analysis of Post-Tensioned Steel Frames against Progressive Collapse.” Eng. Struct. 126: 446–456.

484 Qian, K., Lan, X., Li, Z., Li, Y., and Fu, F. (2020). "Progressive Collapse Resistance of Two-Storey
485 Seismic Configured Steel Sub-Frames Using Welded Connections." J. Constr. Steel Res. 170:
486 106117.
487 Qian, K., Liang, S. L., Fu, F., and Li, Y. (2021a). "Progressive Collapse Resistance of Emulative
488 Precast Concrete Frames with Various Reinforcing Details." J. Struct. Eng. 147(8): 04021107.
489 Qian, K., Lan, X., Li, Z., and Fu, F. (2021b). "Behavior of Steel Moment Frames using Top-and-
490 Seat Angle Connections under Various Column Removal Scenarios." J. Struct. Eng.
491 10.1061/(ASCE)ST.1943-541X.0003089.
492 Richard, R. M. (1986). "Analysis of Large Bracing Connection Designs for Heavy Construction." In
493 Proc., National Steel Construction Conf., 1-24. Chicago: AISC.
494 Ricles, J. M., Sause, R., Garlock, M. M., and Zhao, C. (2001). "Posttensioned Seismic-Resistant
495 Connections for Steel Frames." J. Struct. Eng. 127 (2): 113–121.
496 Sadek, F., Main, J. A., Lew, H. S., and Bao, Y. H. (2011). "Testing and Analysis of Steel and Concrete
497 Beam-Column Assemblies under a Column Removal Scenario." J. Struct. Eng. 137 (9): 881-892.
498 Sadek, F., Main, J. A., Lew, H. S., and El-Tawil, S. (2013). "Performance of Steel Moment
499 Connections under a Column Removal Scenario. II: Analysis." J. Struct. Eng. 139(1):108-119.
500 Tang, H. Y., Deng, X. Z., Jia, Y. G., Xiong, J. G., and Peng, C. M. (2019). "Study on the Progressive
501 Collapse Behavior of Fully Bolted RCS Beam-to-Column Connections." Eng. Struct. 199: UNSP
502 109618.
503 Wang, H., Tan, K. H., and Yang, B. (2020). "Experimental Tests of Steel Frames with Different Beam-
504 Column Connections under Falling Debris Impact." J. Struct. Eng. 146 (1): 04019183.
505 Weng, Y. H., Qian, K., Fu, F., and Fang, Q. (2020). "Numerical Investigation on Load Redistribution
506 Capacity of Flat Slab Substructures to Resist Progressive Collapse." J. Build. Eng. 29: 101109.
507 Yang, B., and Tan, K. H. (2013a). "Experimental Tests of Different Types of Bolted Steel Beam-
508 Column Joints under a Central-Column-Removal Scenario." Eng. Struct. 54: 112-130.

Yang, B., and Tan, K. H. (2013b). "Robustness of Bolted-Angle Connections against Progressive Collapse: Experimental Tests of Beam-Column Joints and Development of Component-Based Models." J. Struct. Eng. 139 (9): 1498-1514.

FIGURE CAPTIONS

Fig. 1. Location of the extracted frame in the prototype building (unit in mm): (a) plan view; (b) elevation view

Fig. 2. Dimensions of the specimen and locations of strain gauge and displacement transducers (unit in mm): (a) arrangements of strain gauges/rosettes and displacement transducers; (b) strain gauges positions on sections

Fig. 3. Geometric details of connections (unit in mm): (a) welded connection; (b) end plate connection; (c) reduced beam section connection

Fig. 4. Test setups of EX: (a) schematic view; (b) photograph

Fig. 5. Vertical force-middle column displacement curves: (a) comparison of WX and WB; (b) comparison of EX and EB; (c) comparison of RV and RB

Fig. 6. Failure mode of WB

Fig. 7. Failure mode of WX

Fig. 8. Failure mode of EB

Fig. 9. Failure mode of EX

Fig. 10. Failure mode of RB

Fig. 11. Failure mode of RV

Fig. 12. Horizontal reaction force-middle column displacement curves: (a) WB; (b) WX; (c) EB; (d) EX; (e) RB; (f) RV

Fig. 13. Horizontal movement of exterior joints: (a) WB; (b) WX

Fig. 14. Schematic diagram of internal force calculation of RV: (a) idealized model; (b) internal forces transformation

Fig. 15. Comparisons of vertical load resistance and horizontal reaction force from strain gauge and load cells: (a) WB; (b) WX

Fig. 16. De-composition of the load resistance from bareframe and steel brace: (a) WX; (b) EX; (c) RV

Fig. 17. Comparison of the behaviour of different connections: (a) vertical force; (b) flexural action; (c) catenary action

Fig. 18. De-composition of the load resistance of bareframe from different actions (Note: FA and CA represent flexural action and catenary action, respectively) : (a) WB; (b) WX; (c) EB; (d) EX; (e) RB; (f) RV

Fig. 19. De-composition of load resistance from 1st story and 2nd story: (a) WB; (b) WX; (c) EB; (d) EX; (e) RB; (f) RV

Fig. 20. Comparisons of the flexural and catenary action variation in 1^{st} story and 2^{nd} stories (Note: FA and CA represent flexural action and catenary action, respectively) : (a) WB; (b) WX; (c) EB; (d) EX; (e) RB; (f) RV

Fig. 21. De-composition of the load resistance of brace from different braces (Note: TB and CB represent tensile brace and compressive brace, respectively) : (a) WX; (b) EX; (c) RV

Fig. 22. Axial force of braces (Note: TB and CB represent tensile brace and compressive brace, respectively) : (a) WX; (b) EX; (c) RV

Table 1-Specimen properties

Test ID	Connection type	Steel brace
WB	Welded connection	Bare frame without braces
WX	Welded connection	Braced frame with X braces
RB	Reduced beam section connection	Bare frame without braces
RV	Reduced beam section connection	Braced frame with V braces
EB	End plate connection	Bare frame without braces
EX	End plate connection	Braced frame with X braces

Table 2-Material properties

Items	Plate thickness (mm)	Yield strength (MPa)	Yield strain	Ultimate strength (MPa)	Ultimate strain	Elongation (%)
Beam flange	8.0	310	0.0019	420	0.0240	12.0
Beam web	5.5	320	0.0021	430	0.0249	13.5
Column flange	10.0	300	0.0019	410	0.0267	14.0
Column web	7.0	295	0.0023	375	0.0242	13.0
Steel brace	4.0	310	0.0021	420	0.0256	12.5

Table 3-Test results

Test ID	U_{YL} (mm)	F_{YL} (kN)	K_{YL} (kN/mm)	U_{UL} (mm)	F_{UL} (kN)
WB	45	147.8	3.3	200	197.5
WX	31	233.9	7.5	382	286.5
EB	42	94.4	2.2	515	255.4
EX	30	148.5	5.0	526	469.8
RB	37	106.8	2.9	468	407.0
RV	30	165.2	5.5	421	356.3

Note: F_{YL} and F_{UL} represent yield load and ultimate load, respectively; U_{YL} and U_{UL} represent displacements corresponding the yield load and ultimate load, respectively; K_{YL} represents initial stiffness corresponding the yield load.

Figure 1 Click here to access/download;Figure;Figure 1.pdf

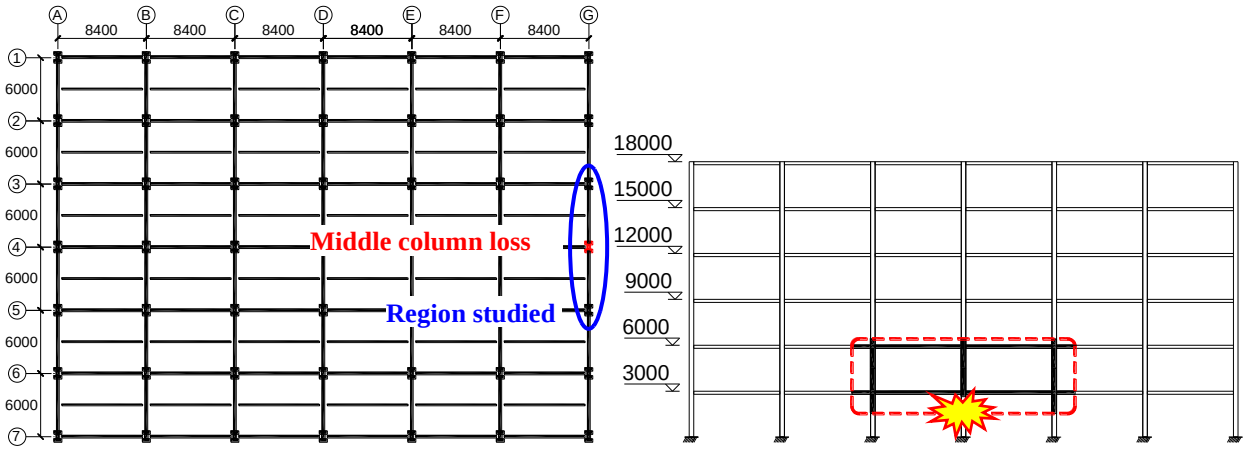

(a) (b)

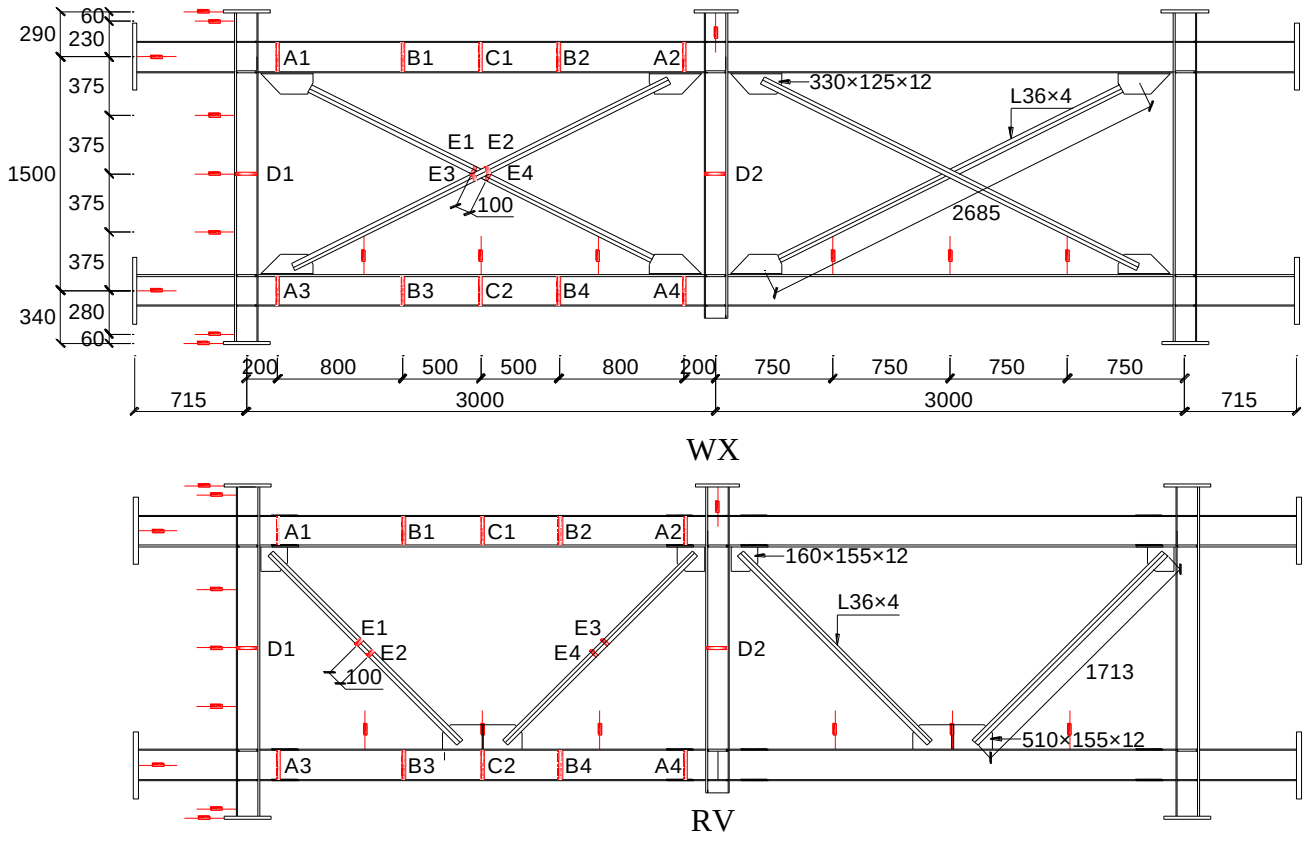

(a)

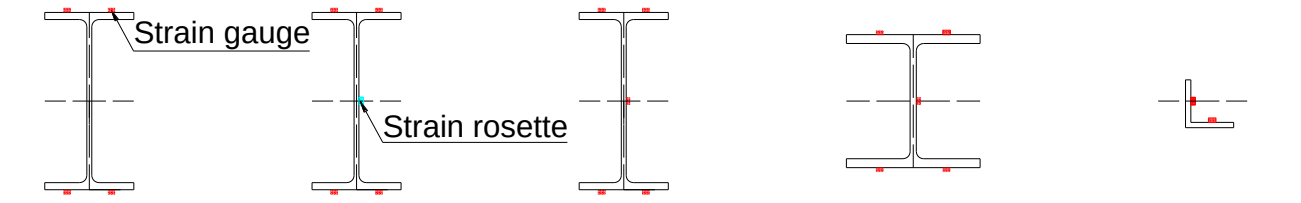

(b)

Figure 3

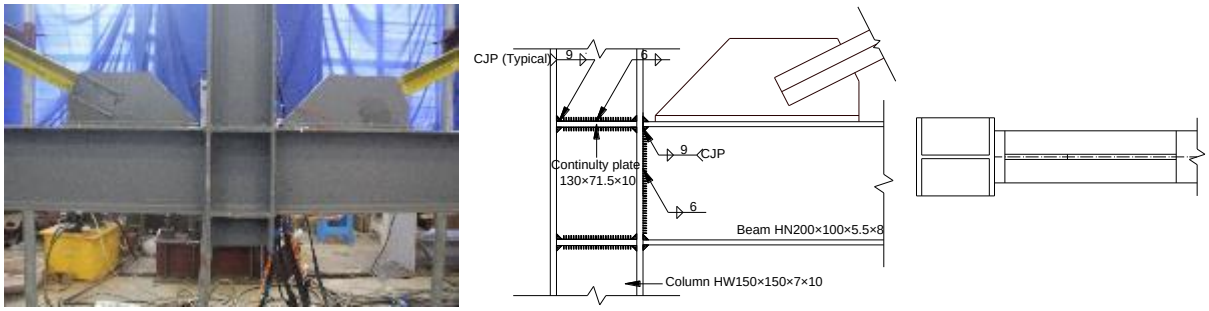

(a)

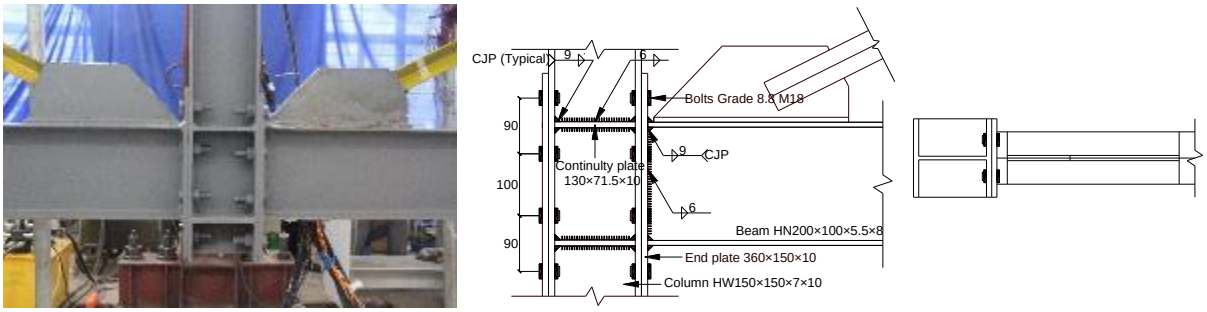

(b)

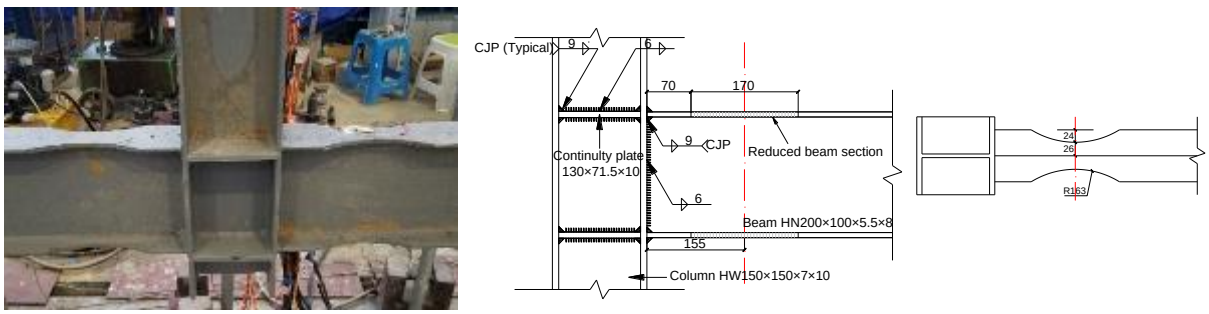

(c)

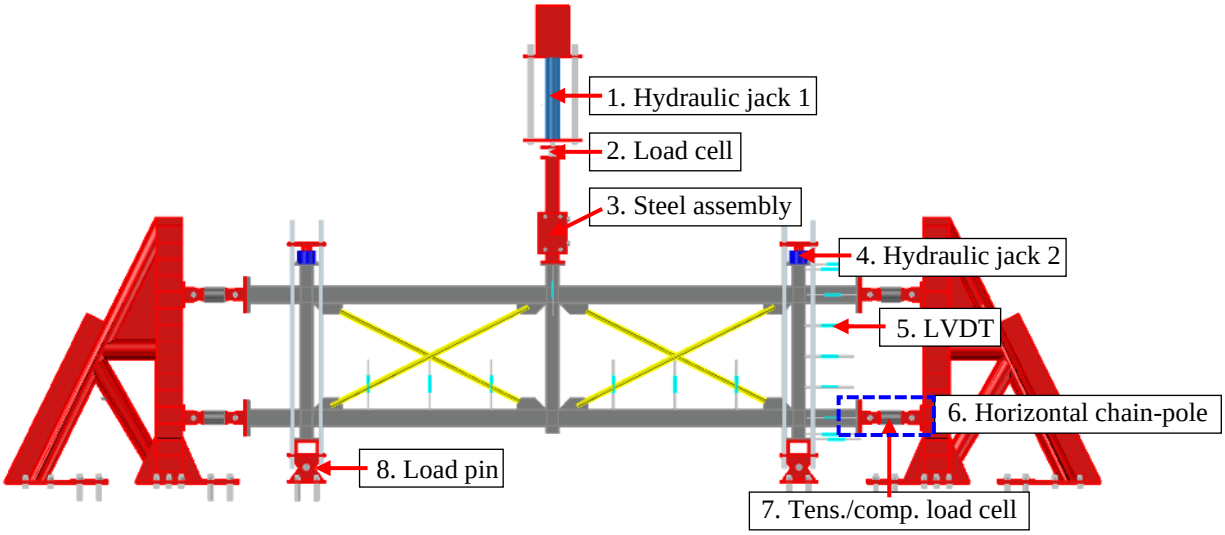

(a)

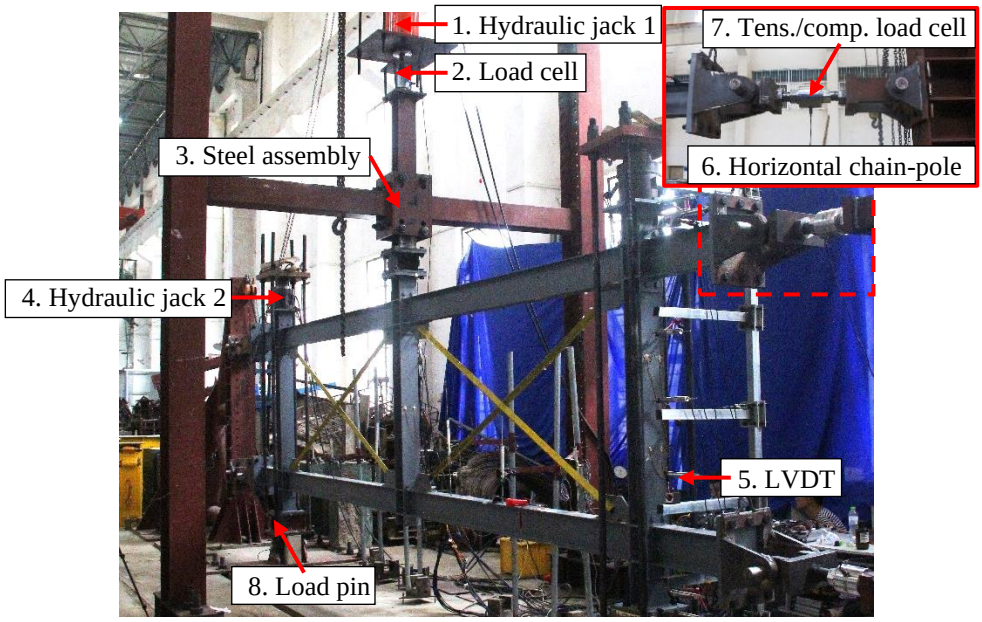

(b)

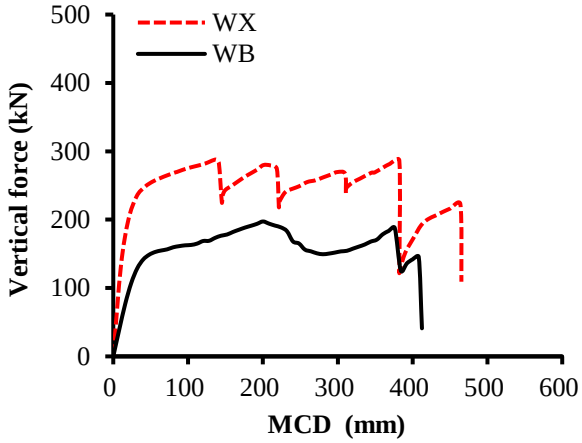

(a)

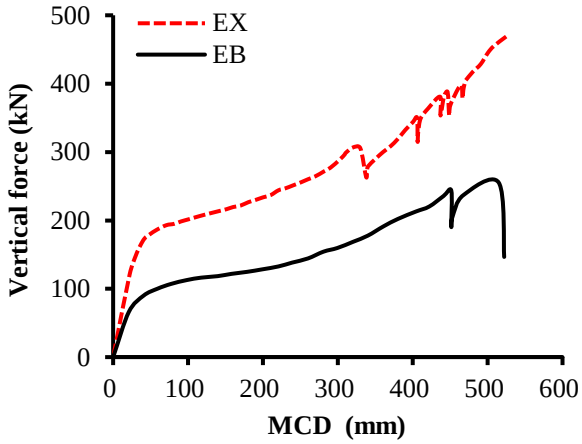

(b)

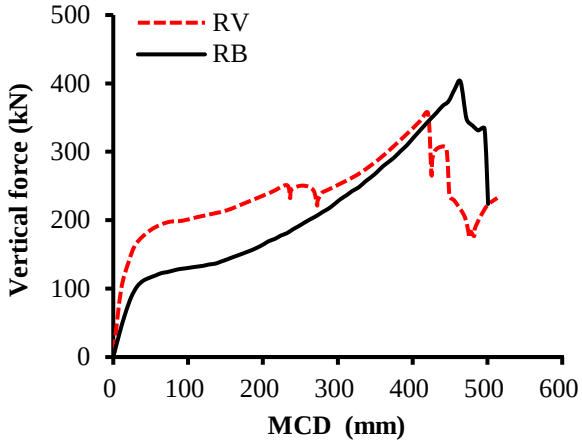

(c)

Figure 6

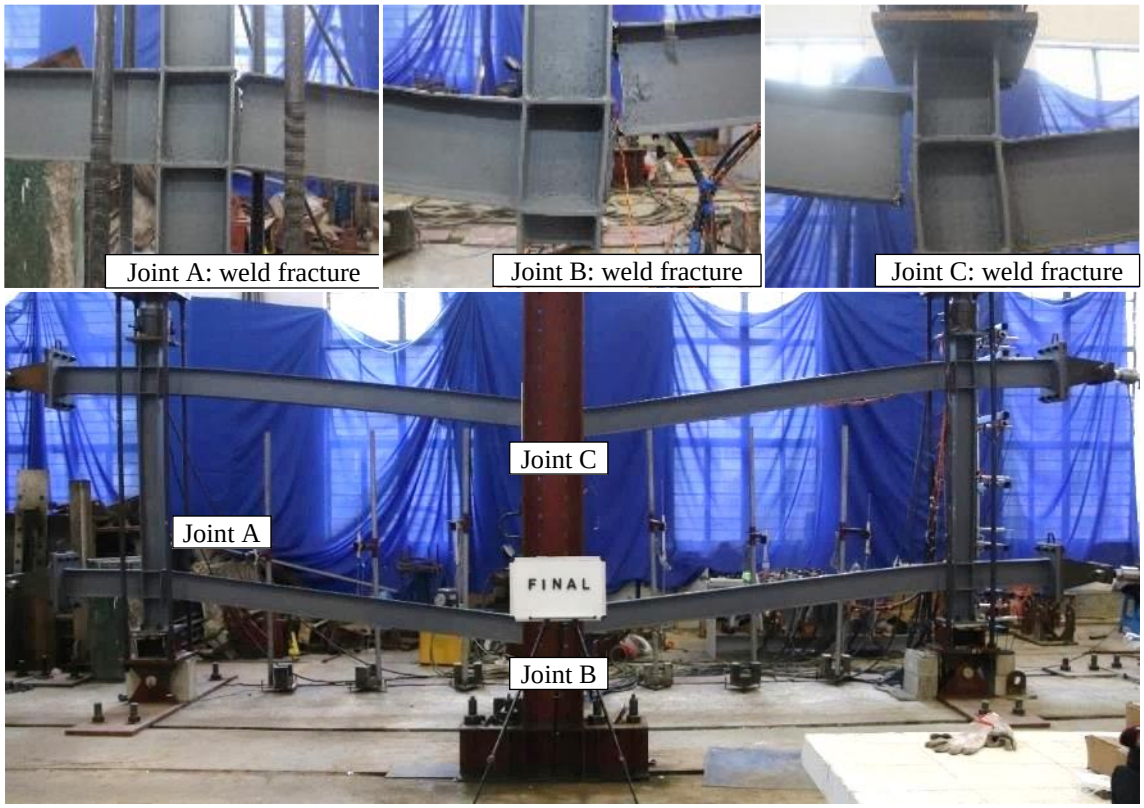

Figure 7

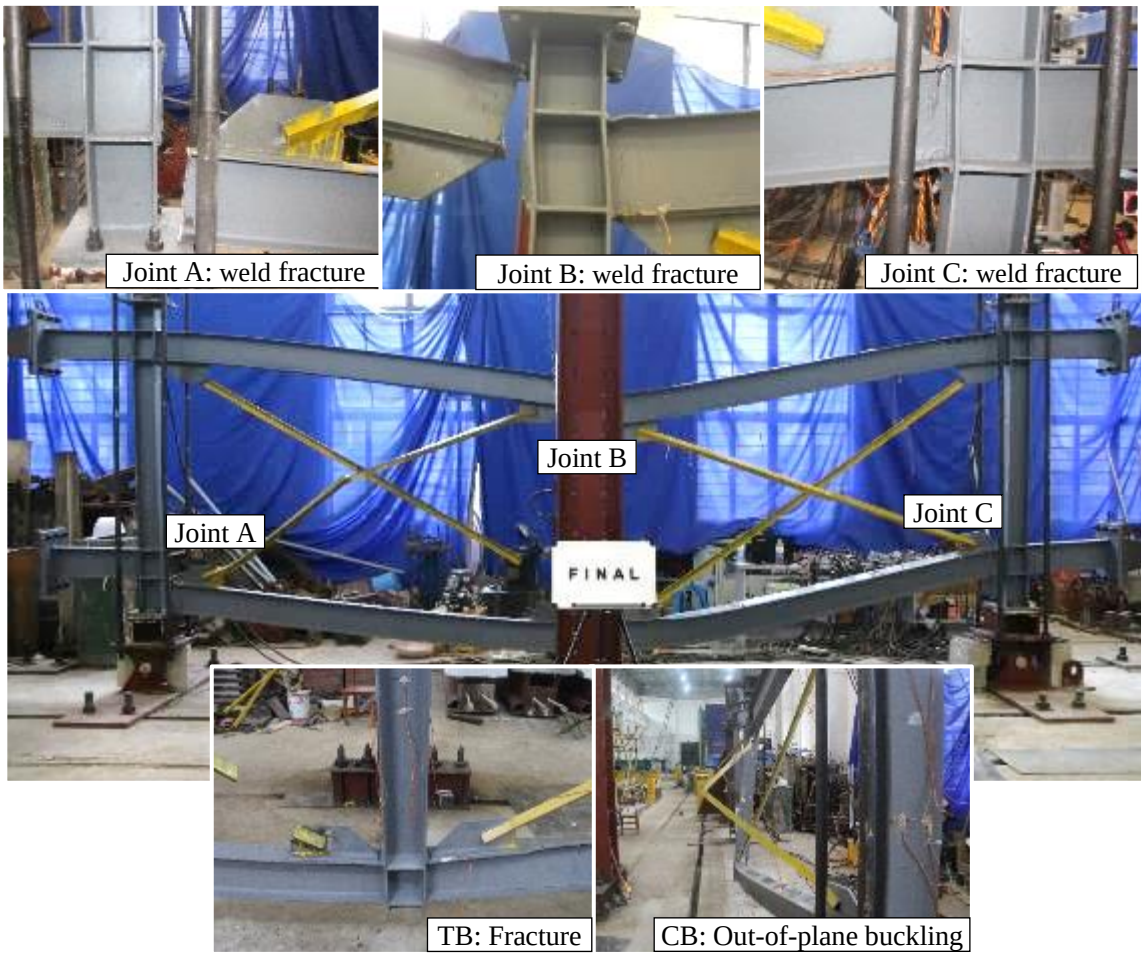

Figure 8

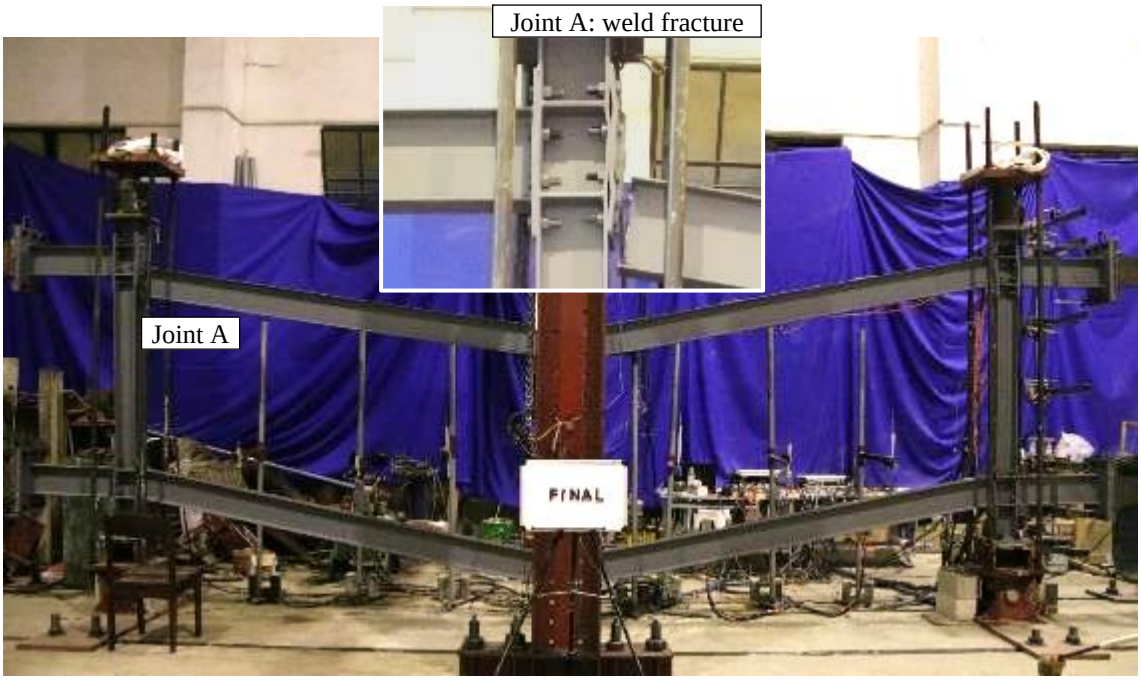

Figure 9

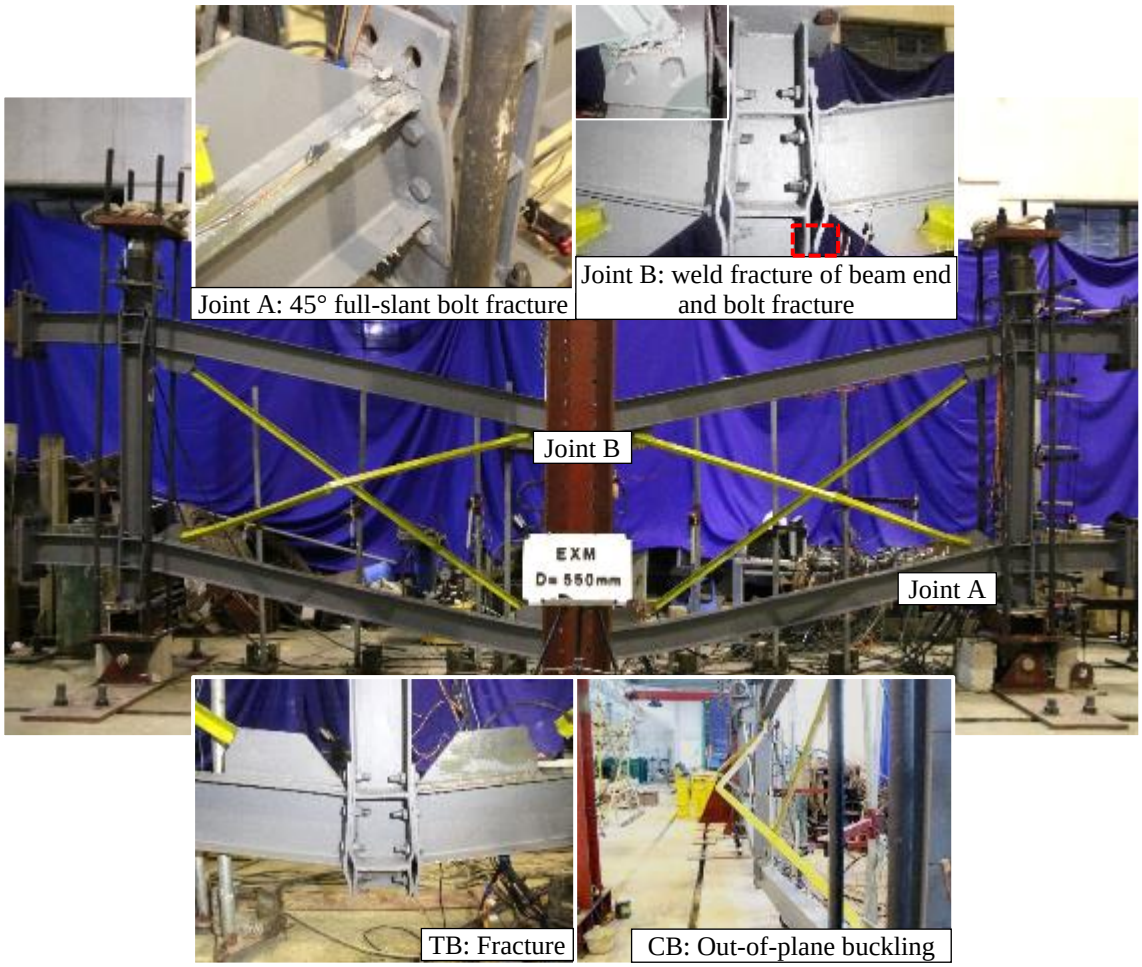

Figure 10

Figure 11

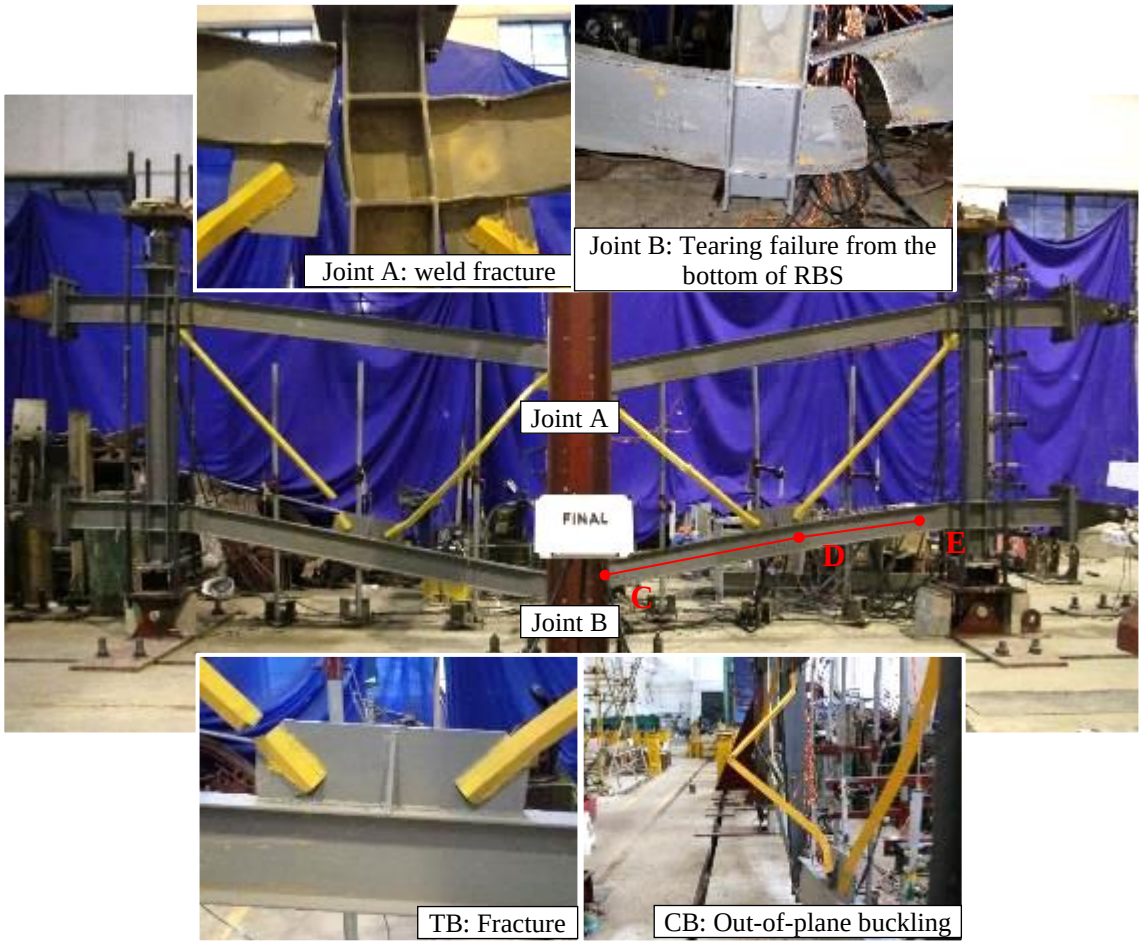

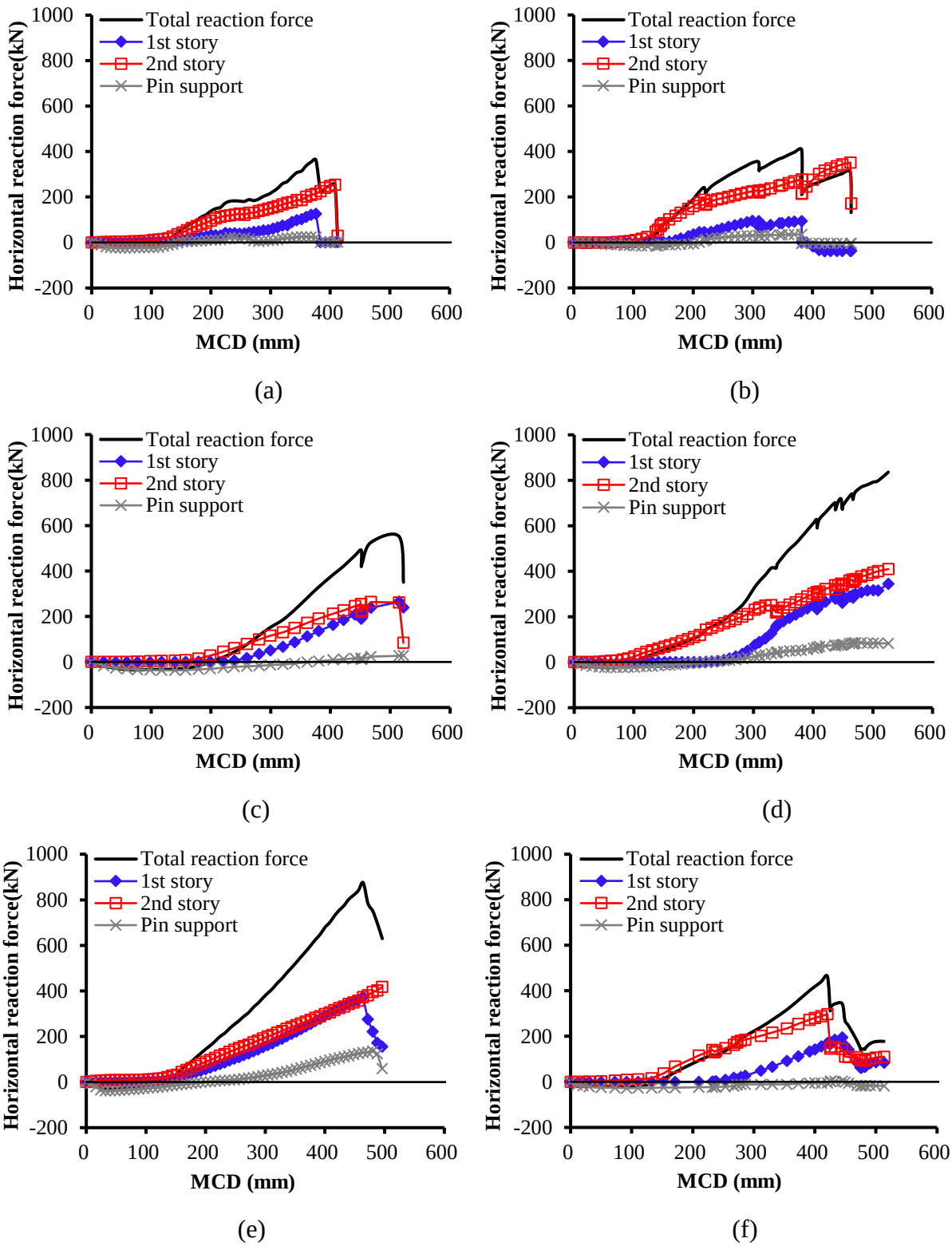

Figure 13

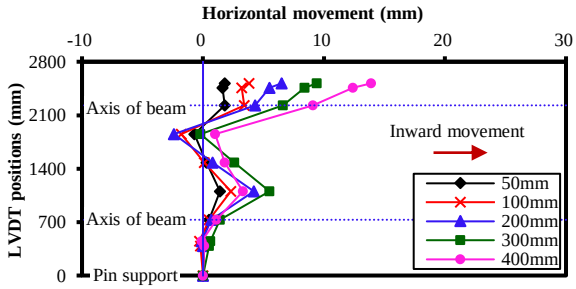

(a)

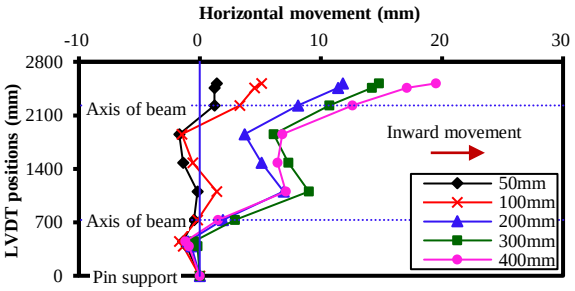

(b)

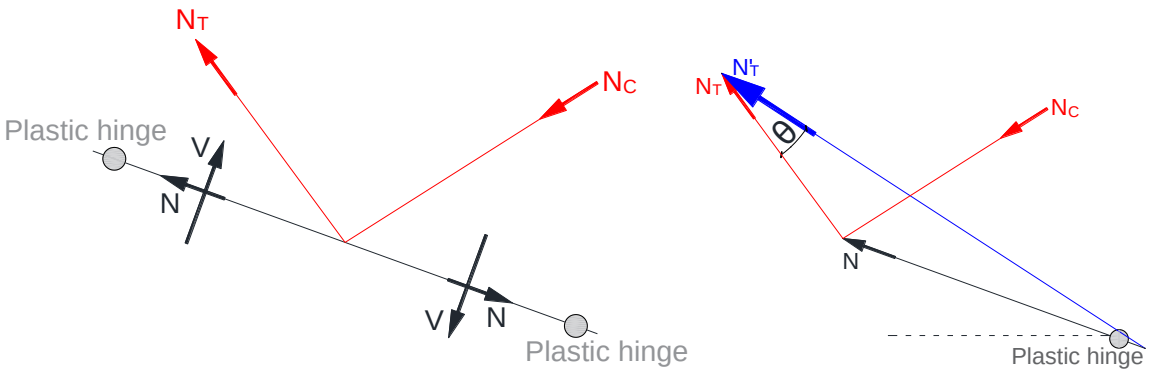

(a) (b)

Figure 15

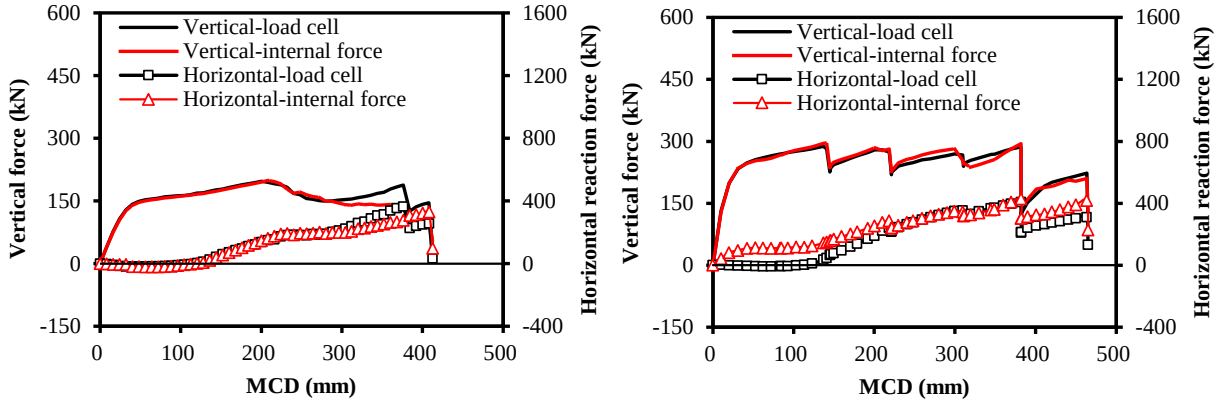

(a) (b)

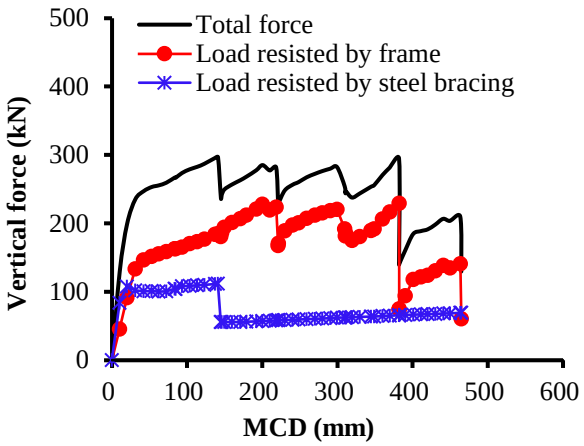

(a)

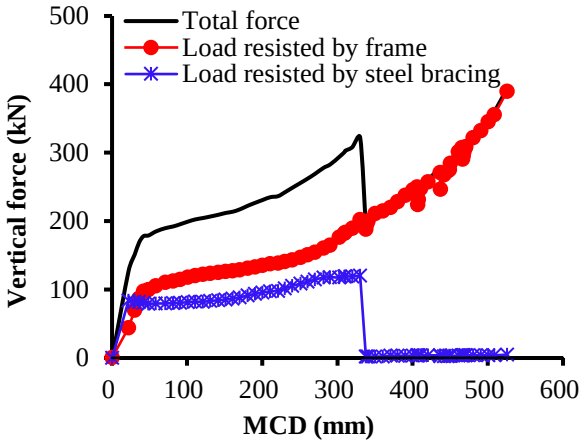

(b)

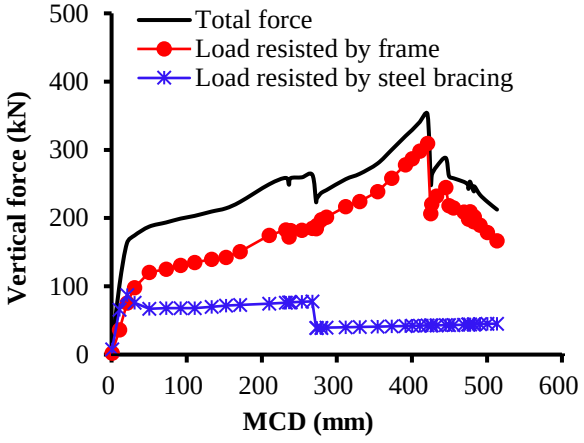

(c)

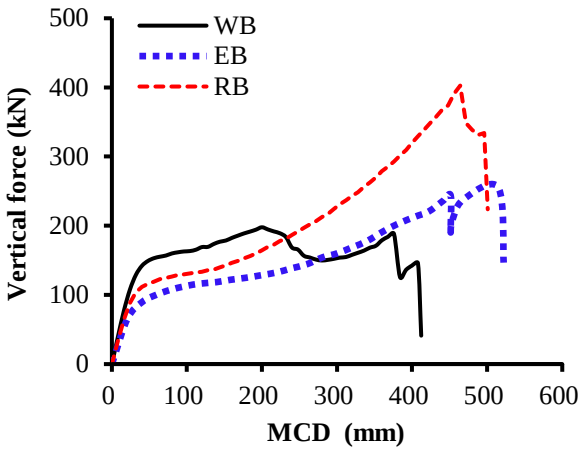

(a)

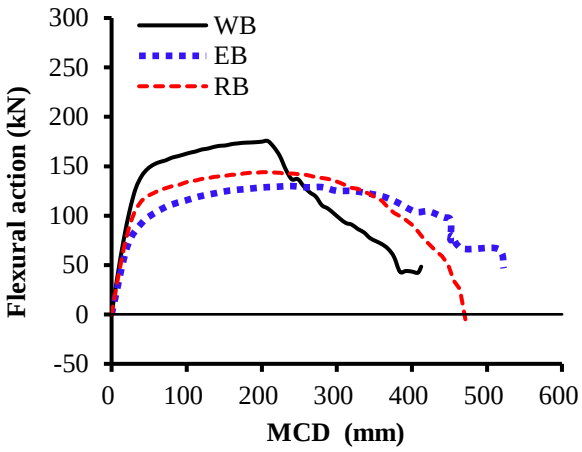

(b)

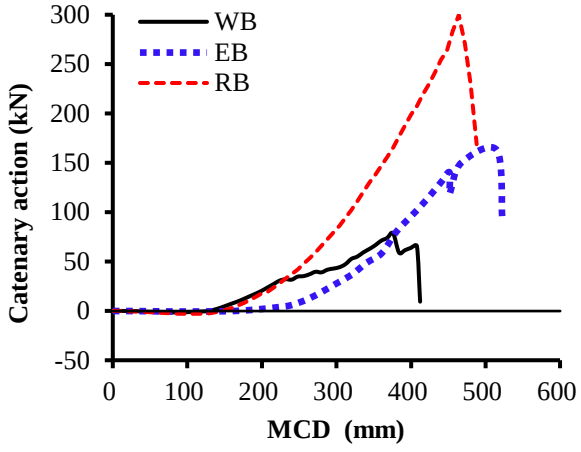

(c)

Figure 18

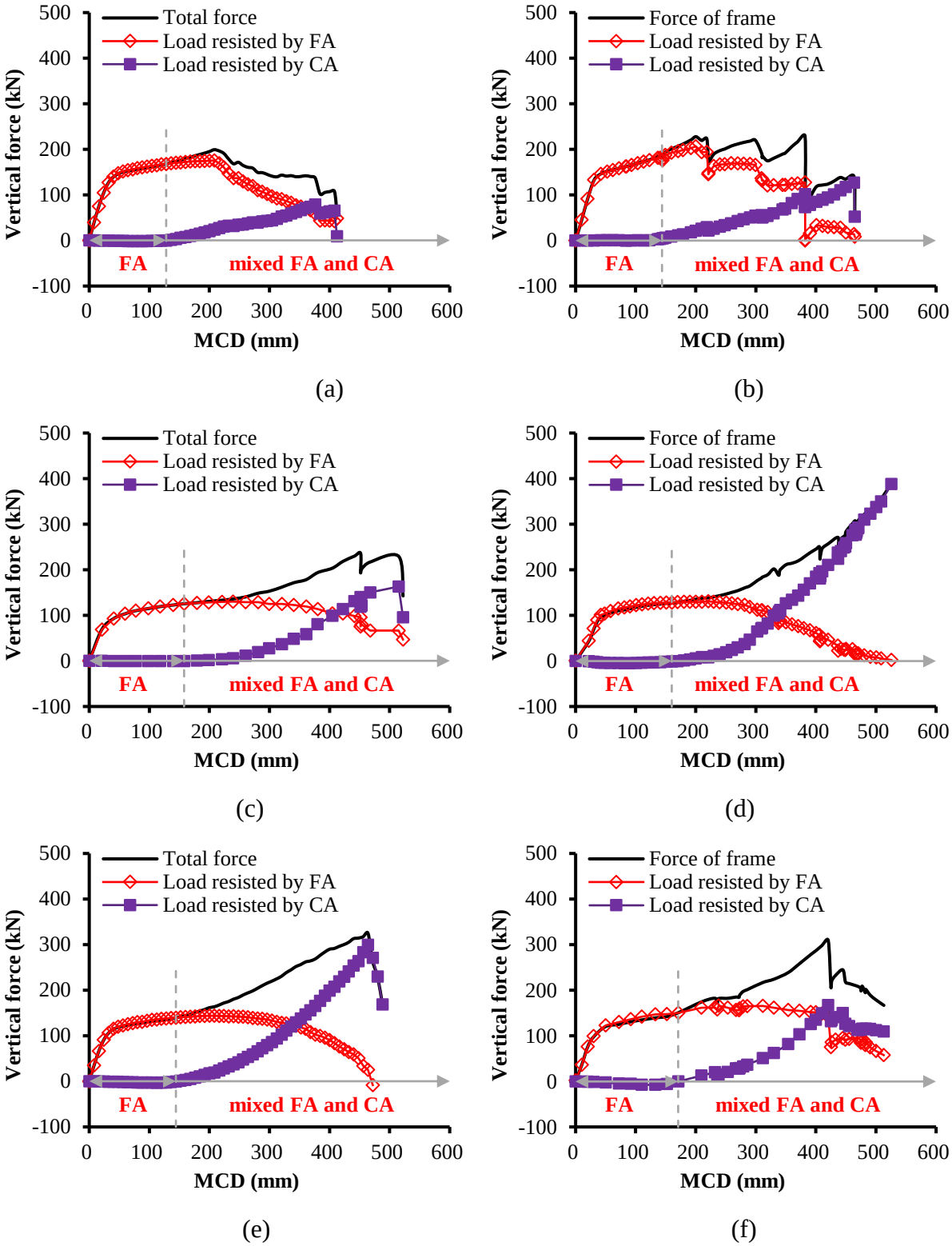

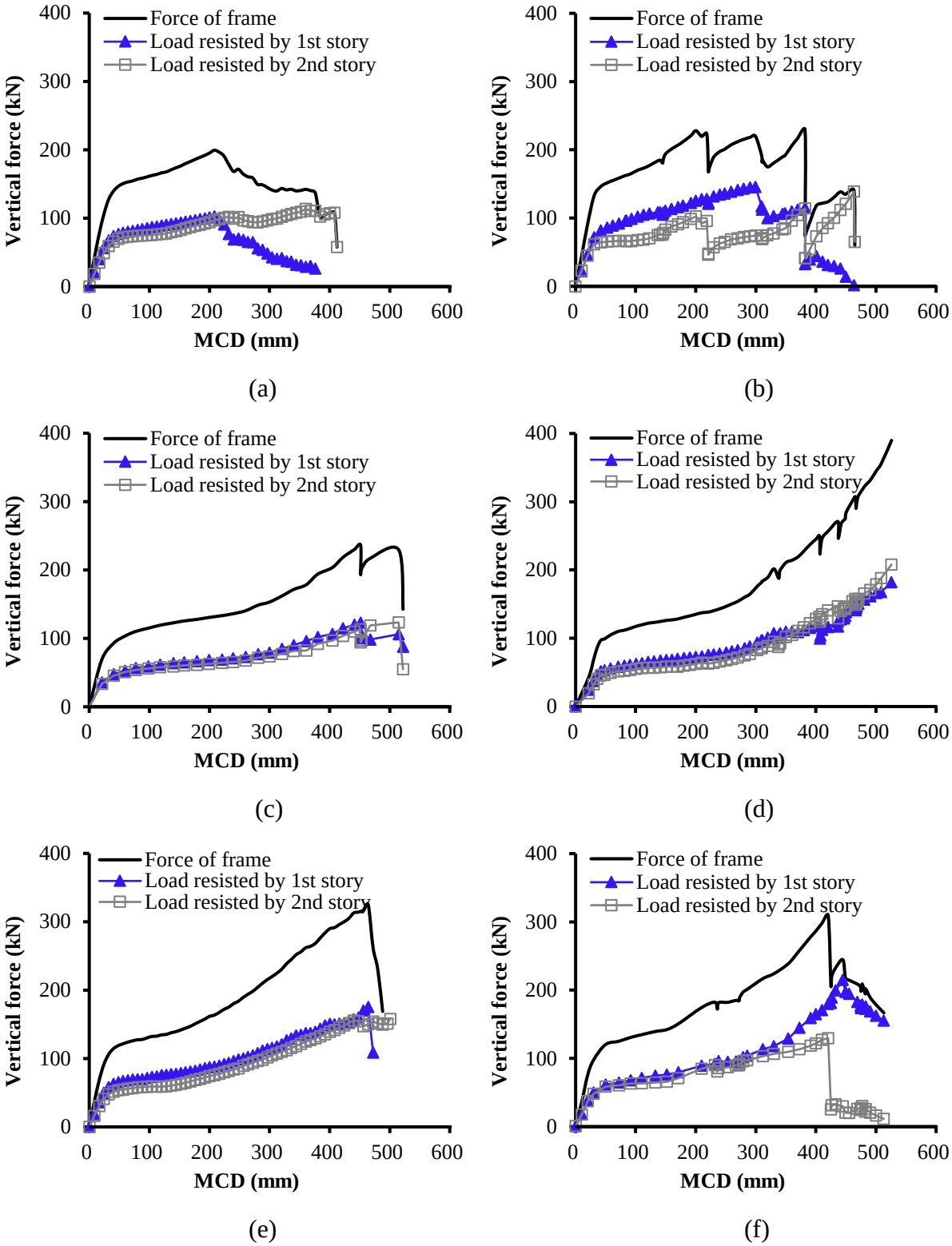

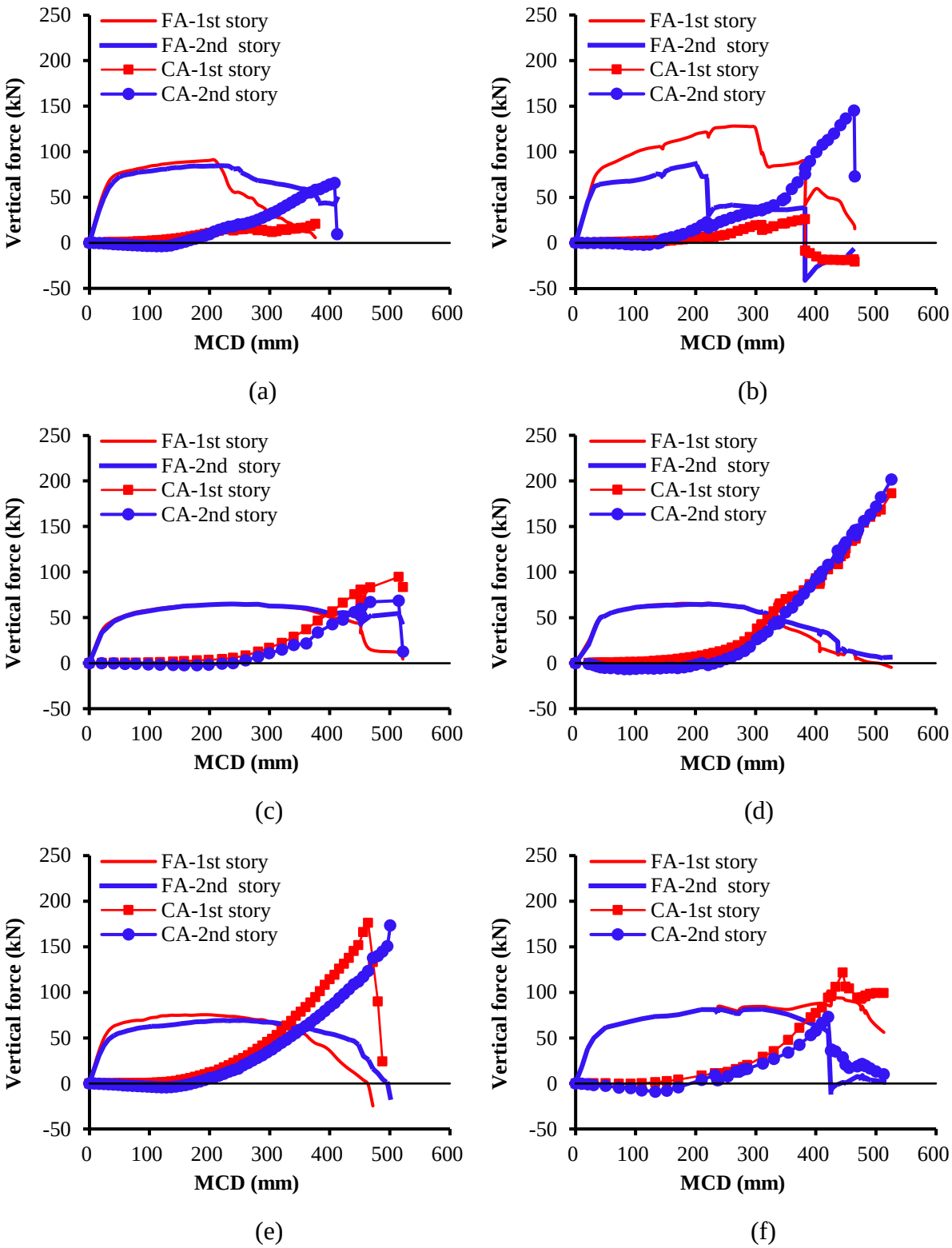

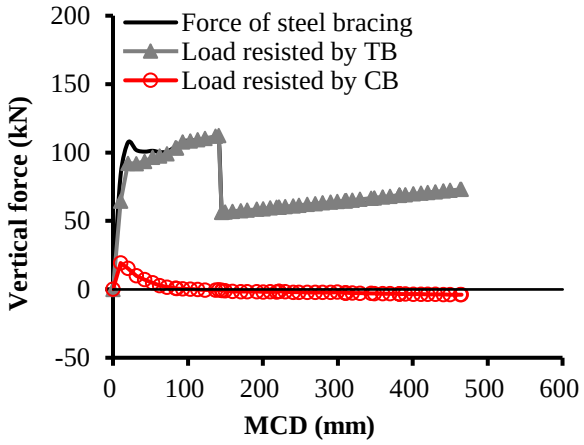

(a)

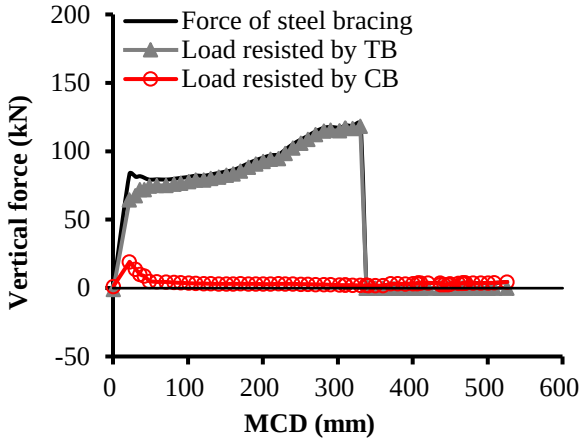

(b)

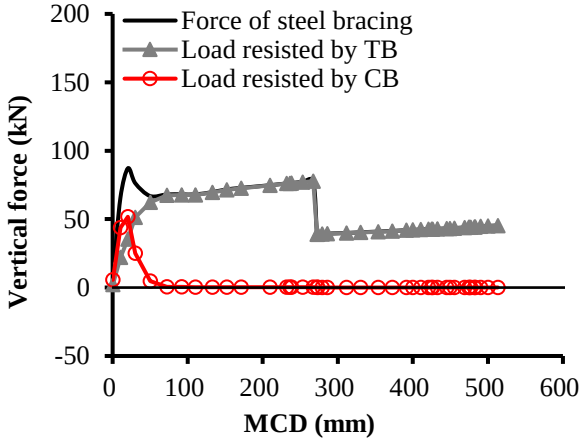

(c)

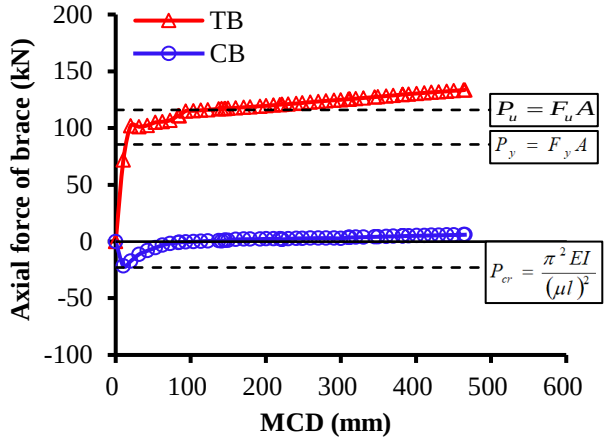

(a)

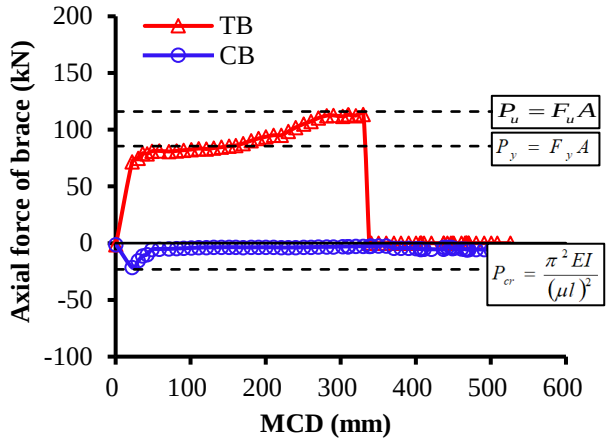

(b)

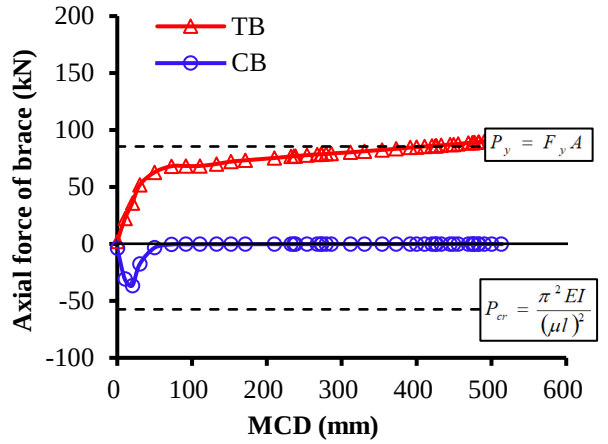

(c)